



Diel-scale variation of dissolved inorganic carbon during a rainfall event in a small karst stream in southern China

Junbing Pu¹ · Jianhong Li¹ · Tao Zhang¹ · Jonathan B. Martin² · Mitra B. Khadka² · Daoxian Yuan¹

Received: 1 October 2018 / Accepted: 3 February 2019 / Published online: 21 February 2019
© Springer-Verlag GmbH Germany, part of Springer Nature 2019

Abstract

Metabolic processes of the submerged aquatic community (photosynthesis and respiration) play important roles in regulating diel cycles of dissolved inorganic carbon (DIC) and sequestering carbon in a karst stream. However, little is known of whether diel DIC cycling occurs during rainfall in a karst groundwater-fed stream, even though this question is critical for the accurate estimation of what may be a major terrestrial carbon sink. Here, we measured diel variations of water chemical composition in a small karst groundwater-fed stream in southwest China during a rainfall event to assess the influences of rainfall and rising discharge on DIC diel cycling and the potential carbon sink produced by in-stream metabolism. Our results show that water chemical composition at the source spring (CK site) is relatively stable due to chemostatic behavior during rising discharge after a rainfall period. This site lacked submerged aquatic vegetation and, thus, had no diel variations in water chemistry. However, diel cycles of all hydrochemical parameters occurred at a site 1.3 km downstream (LY site). Diel variations in pH, DO, and $\delta^{13}\text{C}_{\text{DIC}}$ were inversely related to diel changes in SpC, DIC, Ca^{2+} , and $p\text{CO}_2$. These results indicated that diel cycling of DIC due to in-stream metabolism of submerged aquatic community was still occurring during elevated discharge from rainfall. We estimate the carbon sink through the in-stream metabolism of the submerged aquatic community to be 5.6 kg C/day during the studied rainfall event. These results imply that submerged aquatic communities in a karst stream can significantly stabilize carbon originating from the carbonate rock weathering processes in karst areas.

Keywords Dissolved inorganic carbon · Rainfall · Diel cycle · Carbon sink · In-stream metabolism · Karst stream

Introduction

The World Karst Aquifer Map (WOKAM) project has found that karstified rocks and aquifer systems cover approximately 14.7% of the Earth's ice-free land (Chen et al. 2017). In karst areas, many surface streams are fed by karst groundwaters, which discharge from aquifer at springs. Karst groundwater

is often rich in dissolved inorganic carbon (DIC) because of carbonate dissolution by carbonic acid generated during the hydration of CO_2 . The elevated DIC concentrations may lead karst groundwater-fed streams to play an important role in regulating regional and global carbon cycles through carbon transfer, CO_2 degassing, carbon burial, and carbon assimilation (Atekwana and Krishnamurthy 1998; Covington 2016; Gombert 2002; Jiang and Yuan 1999; Kurz et al. 2013; Liu et al. 2010, 2015; Liu and Zhao 2000; Martin 2017; Martin et al. 2013; Pu et al. 2017; Yuan 1997). In particular, these streams may represent an important carbon sink, as the clear water allows light penetration to stream benthic environments and DIC is assimilated by submerged aquatic phototrophs (de Montety et al. 2011; Jiang and Yuan 1999; Liu and Dreybrodt 2015; Liu et al. 2010; Pu et al. 2017; Zhang et al. 2017a). The assimilated DIC is then buried and sequestered as organic carbon (OC). The net atmospheric CO_2 uptake by interactions between water, carbonate minerals, dissolved CO_2 (carbonic acid), and aquatic phototrophs on land has been estimated to be as large as 0.477 Pg C/a (Liu and Dreybrodt 2015), and thus a large fraction of the net terrestrial residual sink (i.e.,

Responsible editor: Philippe Garrigues

Electronic supplementary material The online version of this article (<https://doi.org/10.1007/s11356-019-04456-z>) contains supplementary material, which is available to authorized users.

✉ Junbing Pu
junbingpu@karst.ac.cn

¹ Key Laboratory of Karst Dynamics, MNR & Guangxi, Institute of Karst Geology, Chinese Academy of Geological Sciences, Guilin 541004, China

² Department of Geological Sciences, University of Florida, Gainesville, FL 32611, USA

0.8–1.2 Pg C/year) (Ciais et al. 2013). Therefore, revealing DIC dynamics in karst streams is critical to understanding carbon cycling and its role in regional and global carbon budgets.

Karst aquifers are very sensitive to external environmental changes at a range of timescales, including diel, event, seasonal, annual, and multi-annual (Liu et al. 2015, 2007; Martin et al. 2016; Nimick et al. 2011; Shuster and White 1971; Vesper and White 2004; Zhang et al. 2012). Thus, DIC in karst groundwater-fed streams can display high temporal and spatial variability in coherence with aquifer hydrological variations (Zeng et al. 2016). Diel variations in DIC concentrations is a common phenomenon in a karst stream that results from alternating carbonate dissolution and aquatic metabolism (de Montety et al. 2011; Demars et al. 2015; Khadka et al. 2014; Lynch et al. 2010; Spiro and Pentecost 1991; Tobias and Boehlke 2011). These diel variations occur in all seasons, and they can be as large as seasonal variations (Nimick et al. 2011). Variations in stream flow may also play an important role in regulating karst stream DIC transport and transformation at diel, seasonal, and annual timescales (Atkins et al. 2017; Peter et al. 2014; Zeng et al. 2016). Dry seasons often slow water motion in channels and increase the time available for DIC transformations through mineral precipitation and plant assimilation (Mann et al. 2014; Shin et al. 2011). By contrast, rainfall events during wet season can export significant quantities of DIC from karst aquifer to surface streams, thereby altering the DIC cycling through changes to CO₂ gas exchange, turbidity, water temperature, and flow velocity (Looman et al. 2016; Peter et al. 2014). The control of changing flow conditions was poorly constrained, however, because most earlier work occurred during lower-water-level or stable flow periods (de Montety et al. 2011; Jiang et al. 2013; Liu et al. 2015; Parker et al. 2014; Pu et al. 2017; Yang et al. 2015). Only a few studies have reported on DIC or the CO₂ diel cycle under the impact of rainfall events in surface streams (Dinsmore et al. 2013; Johnson et al. 2009; Looman et al. 2016; Peter et al. 2014), but they mostly focused on peatland or silicate rock streams. Little is known of how flow variations may alter diel DIC cycling in a karst stream, even though this question is critical for the accurate estimation of what may be a major terrestrial carbon sink.

This study assesses DIC concentration variations during changing flow conditions and how the variations may alter the carbon cycle in a karst system. This assessment is based on data collected from a subtropical karst groundwater-fed stream (Guancun stream (GS)) located in southwest China. The study is based on a 3-day record of high-resolution measurements of diel variations within a stream of water for DIC concentrations, $\delta^{13}\text{C}_{\text{DIC}}$ values, and physicochemical parameters. These results will help to improve evaluations of the amount of carbon that could be sequestered in karst streams and improve the understanding of carbon transportation and

transfer with varying hydrological processes in inland water bodies.

Study area

The Guancun surface stream (GSS) is a tributary of the Shimen River and a part of the Rongjiang River drainage system, which is located in Daliang town in Rong'an county of Guangxi Zhuang Autonomous Region, China (Fig. 1). GSS is a typical subtropical headwater stream and almost entirely fed by karst groundwater from an upper Devonian (D_{3r}) limestone aquifer (Pu et al. 2017). The outlet of the Guancun underground stream (GUS) is the head of the GSS with no surface tributaries flowing into it (Fig. 1). The GSS channel is underlain by Lower Carboniferous (C1y) limestone interbedded with dolomite of the Yingtang Formation. The length and average width of the GSS are 1.32 km and 3.5 m, respectively. At base level, the water depth is shallow (0.2–1.2 m). The study area is characterized by a cold–dry winter from late November through March and a hot–rainy summer from April through October and has an annual average temperature of 19.7 °C. The area is dominated by the East Asian Monsoon with an annual average precipitation of 1726 mm, 72% of which occurs in the wet season from late April to early September. As a typical monsoon region, air temperature and precipitation in the GSS catchment co-vary, both of which being high in the wet season and low in the dry season.

This study focuses on monitoring sites for detailed diel monitoring and sampling (Fig. 1). The upstream CK (24° 52' 10", 109° 20' 07") site is located at a GUS outlet, which receives typical karst groundwater. The downstream LY (24° 51' 32", 109° 20' 01") site is approximately 1.30 km downstream from CK near the stream mouth and is the site of a gauging station.

Methods

Data for this study was acquired August 17–19, 2013. Two multi-parameter meters (WTW 3430, WTW GmbH, Weilheim, Germany) were set at both the CK and LY sites. Hydrochemical variables including water temperature, pH, dissolved oxygen (DO), and specific conductivity (SpC) were continuously measured in situ at 15-min time intervals at both sites. Resolutions for water temperature, pH, dissolved oxygen (DO), and specific conductivity (SpC) are 0.1 °C, 0.004 pH units, 0.01 mg/L, and 1 $\mu\text{S}/\text{cm}$, respectively. Specific conductivity (SpC) refers to the electrical conductivity corrected from ambient temperature to 25 °C by a nonlinear correction function. Turbidity was measured in situ at 15-min time intervals at the LY site using a YSI 6600 datasonde (Yellow Springs, OH, USA). All monitoring probes for the instruments

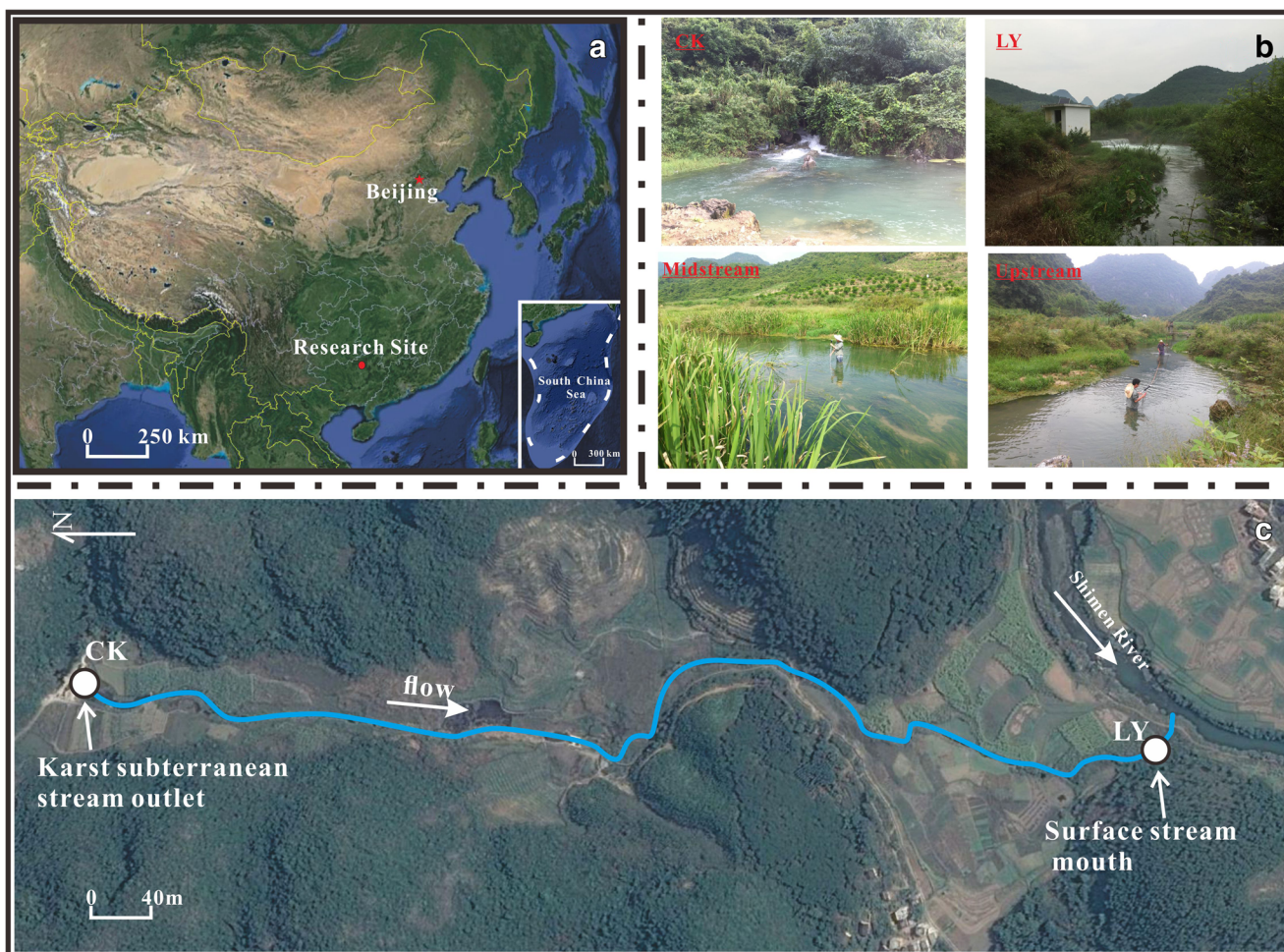


Fig. 1 Maps of Guancun surface stream and sampling sites. **a** Photograph is the location of Guancun stream in SW China. **b** Photographs are the scenes in Guancun stream from groundwater outlet to stream mouth. **c**

Map shows the surface stream flow route and sampling sites in study area (modified from Google Earth 2015) (Pu et al. 2017)

were calibrated according to manufacturer’s specifications prior to deployment. Weir water stages were also continuously monitored at 15-min time intervals at the LY site using the same YSI 6600 datasonde. These water stage measurements were converted to discharge units using the rectangular-weir-discharge formula (Pu et al. 2017).

From August 17 to 19, 2013, water samples were collected every 2 h at both sites from the mid-channel of the stream using the ISCO 6712 autosampler (Teledyne ISCO, Inc., USA). Water was pumped from 0.1 m below the water surface. Every water sample was temporarily stored in 2-L pre-rinsed high-density polyethylene (HDPE) bottles in the autosampler base after samplings. To keep water samples chilled, the autosampler base was filled with ice for entire sampling time. Unfiltered water samplers were titrated for alkalinity immediately in the field with an accuracy of 0.05 mmol/L using a portable testing kit by Merck KGaA Co. (Germany). Because HCO_3^- constitutes ~90% of DIC over the pH range of 7.3–8.5 (Rice et al. 2012), we used alkalinity measurements as an approximation of DIC concentration for this study. Water from the

autosampler bottles was immediately filtered (0.45- μm cellulose acetate membrane) into other small clean bottles for later analysis of major cation (Ca^{2+} , Mg^{2+} , K^+ , and Na^+), major anions (Cl^- , SO_4^{2-}), and $\delta^{13}\text{C}_{\text{DIC}}$. Samples used to detect cations were acidified with trace metal grade nitric acid (7 M HNO_3) to a pH of <2.0. Samples for $\delta^{13}\text{C}_{\text{DIC}}$ were collected in 25-mL acid-washed dry HDPE bottles, and three drops of HgCl_2 were added in order to prevent microbial activity. A portable cooler was used to store all samples in the field. Samples were delivered to a laboratory where they were stored and chilled in a refrigerator at 4 °C until analysis.

Meteorological parameters, including rainfall, air temperature, wind speed, barometric pressure, and solar radiation, were measured using an on-site Vantage Pro 2 weather station (Davis Instruments Corp., USA) from August 16 to 20, 2013. Resolutions of rainfall, air temperature, wind speed, barometric pressure, and solar radiation were 0.2 mm, 0.1 °C, 5%, 0.1 hPa, and 1 W/m^2 , respectively.

Major anions and cations were measured by an automated Dionex ICS-900 ion chromatograph and an ICP-OES (IRIS

Intrepid II XSP, Thermo Fisher Scientific, USA), respectively, using procedures based on APHA 2012 methods (Rice et al. 2012). The calculated errors of charge balance were within $\pm 5\%$. The $\delta^{13}\text{C}_{\text{DIC}}$ values of water samples were analyzed using a MAT-253 mass spectrometer coupled with a Gas Bench II automated device. The results are expressed as $\delta^{13}\text{C}_{\text{DIC}} (\text{‰})$ with respect to the Vienna Pee Dee Belemnite (V-PDB) standard with an analytical precision of $\pm 0.15\text{‰}$. All lab analyses were carried at the Environmental and Geochemical Analysis Laboratory of the Institute of Karst Geology, Chinese Academy of Geological Science (Pu et al. 2017; Zhang et al. 2017a).

The partial pressure of CO_2 ($p\text{CO}_2$) and saturation index of calcite (SIc) in the stream waters were calculated through the program WATSPEC (Wigley 1977) according to the hydrochemical data sets, including pH, water temperature, and concentrations of K^+ , Na^+ , Ca^{2+} , Mg^{2+} , Cl^- , SO_4^{2-} , and HCO_3^- .

CO_2 fluxes across water–air interface were calculated using a molecular diffusion model (Raymond et al. 2012):

$$F = k \times ([\text{CO}_2]_{\text{water}} - [\text{CO}_2]_{\text{air}}) \quad (1)$$

where F is the CO_2 evasion flux ($\text{mg}/\text{m}^2/\text{h}$) between water and atmosphere, k is the gas transfer velocity (cm/h), and $[\text{CO}_2]_{\text{water}} - [\text{CO}_2]_{\text{air}}$ is the CO_2 concentration gradient between the water and air. Previous studies measured atmospheric CO_2 concentrations 1.5 m above the water surface that is to be 445 ppmv (Mo 2015). k is a key parameter for accurately calculating CO_2 evasion flux. We calculated k using the temperature-dependent Schmidt number (Sc_T) for freshwater:

$$k = k_{600} \times (Sc_T/600)^{-0.5} \quad (2)$$

with

$$Sc_T = 1911.1 - 118.11T + 3.4527T^2 - 0.04132T^3 \quad (3)$$

where k_{600} is the k for CO_2 at 20°C in freshwater, that is, k at a Schmidt number of 600 (Raymond et al. 2012), and T is the in situ water temperature ($^\circ\text{C}$). k_{600} was derived using an equation described by Raymond et al. (2012):

$$k_{600} = 4725 \times (v \times S)^{0.86} \times Q^{-0.14} \times D^{0.66} \quad (4)$$

where v is the velocity (m/s), S is the channel slope (m/km), Q is the stream discharge (m^3/s), and D is the water depth (m).

Results

Hydrological and meteorological variations

There were some sporadic rain events with a total rainfall of 0.8 mm on the afternoon of August 17, 2013, which did not raise the GSS water level. During the study period, a

concentrated rainfall of ~ 22.8 mm fell from 0700 to 1345 h on August 18, 2013 at an average intensity of 3.38 mm/h and increased the discharge from the base flow value of 20.34 to 83.91 L/s (Figs. 2 and 3). Discharge in GSS is usually controlled by groundwater discharge at GUS outlet (Pu et al. 2017) and had a mean discharge of 46.13 L/s and median of 55.28 L/s during this study (Figs. 2 and 3). Discharge rose quickly in response to the rain event approximately 2.0 h after the rain started. The discharge of GSS was elevated following the peak discharge for the remainder of the study. Turbidity increased after rainfall coincident with the increased discharge, showing two peaks, but a 2-h lagging discharge (Figs. 2 and 3).

Hydrochemical variations

At the CK site, the coefficient of variation (CV) for all measured parameters was very small during the study period. The CV of pH, water temperature, and DO are 0.23%, 0.28%, and 0.16%, respectively, indicating a minor variation during the study period. However, SpC exhibited relatively larger variations, although still small, with a range of 435.0 to 470 $\mu\text{S}/\text{cm}$ with a CV of 2.4% (Fig. 2, Table S1). DIC and Ca^{2+} varied from 278.8 to 287.2 mg/L and 81.0 to 86.1 mg/L with CV values of 0.87% and of 1.7%, respectively (Table S1). Minor variations also occurred in $p\text{CO}_2$ with a CV of 3.9%. Water at CK was supersaturated with respect to calcite, with SIc values ranging from 0.08 to 0.14, with an average value of 0.10. The observed small CV for all the measured parameters at CK suggests no distinct diel variations during the study period (Fig. 2). Although the discharge of GSS quickly rose in response to rainfall, hydrochemical parameters at CK (GUS outlet) show a relative steady status with little storm effect, piston effect, or dilution as can commonly occur in some karst springs (Hess and White 1988; Liu et al. 2004, 2007; Pu et al. 2014; Vesper and White 2003a, b). The small variations appear to reflect chemostatic behavior in the GUS during the rain event (Clow and Mast 2010; Godsey et al. 2009; Karis et al. 2016).

At the LY site, water temperature, SpC, pH, DO, Ca^{2+} , DIC, $p\text{CO}_2$, and SIc values showed pronounced temporal variations during the study period (Fig. 3). The mean stream water temperature was 23.1°C , with a range from 22.3°C just prior to dawn to 24.0°C in the afternoon, consistent with, but slightly lagging with, solar radiation and air temperature variations (Fig. 3). Changes in pH were temporally coincident with changes in DO, with peaks occurring in the afternoon (14:00–16:00) (Fig. 3). pH ranged from a high of 8.11 during the day to a low of 7.99 at night with a mean of 8.05. DO varied from 7.51 mg/L during the day to 6.56 mg/L at night with a mean of 7.18 mg/L. Notably, the pH and DO maxima roughly coincided with the peak of discharge but had an approximate 2-h lag. The temporal pattern of SpC showed an

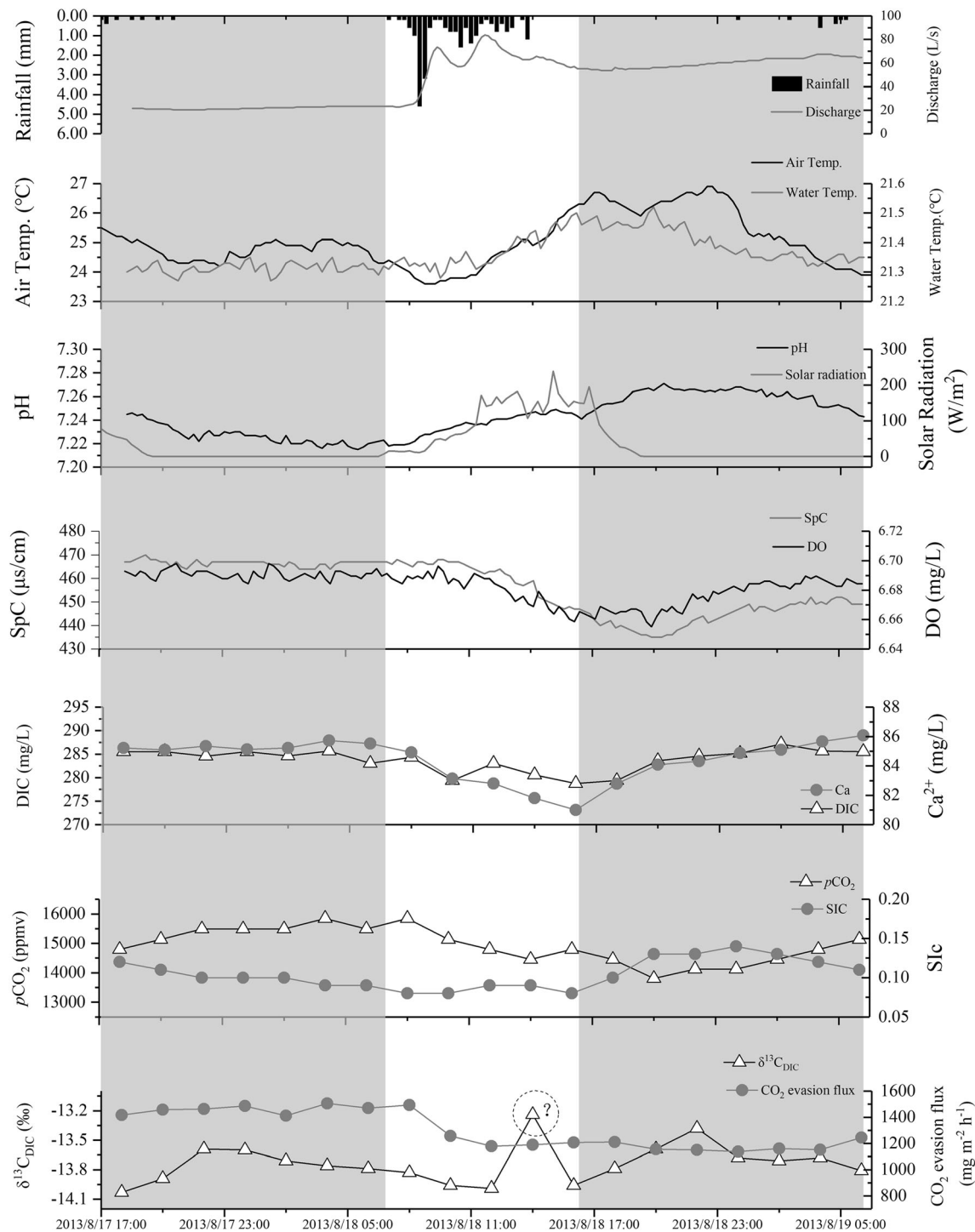


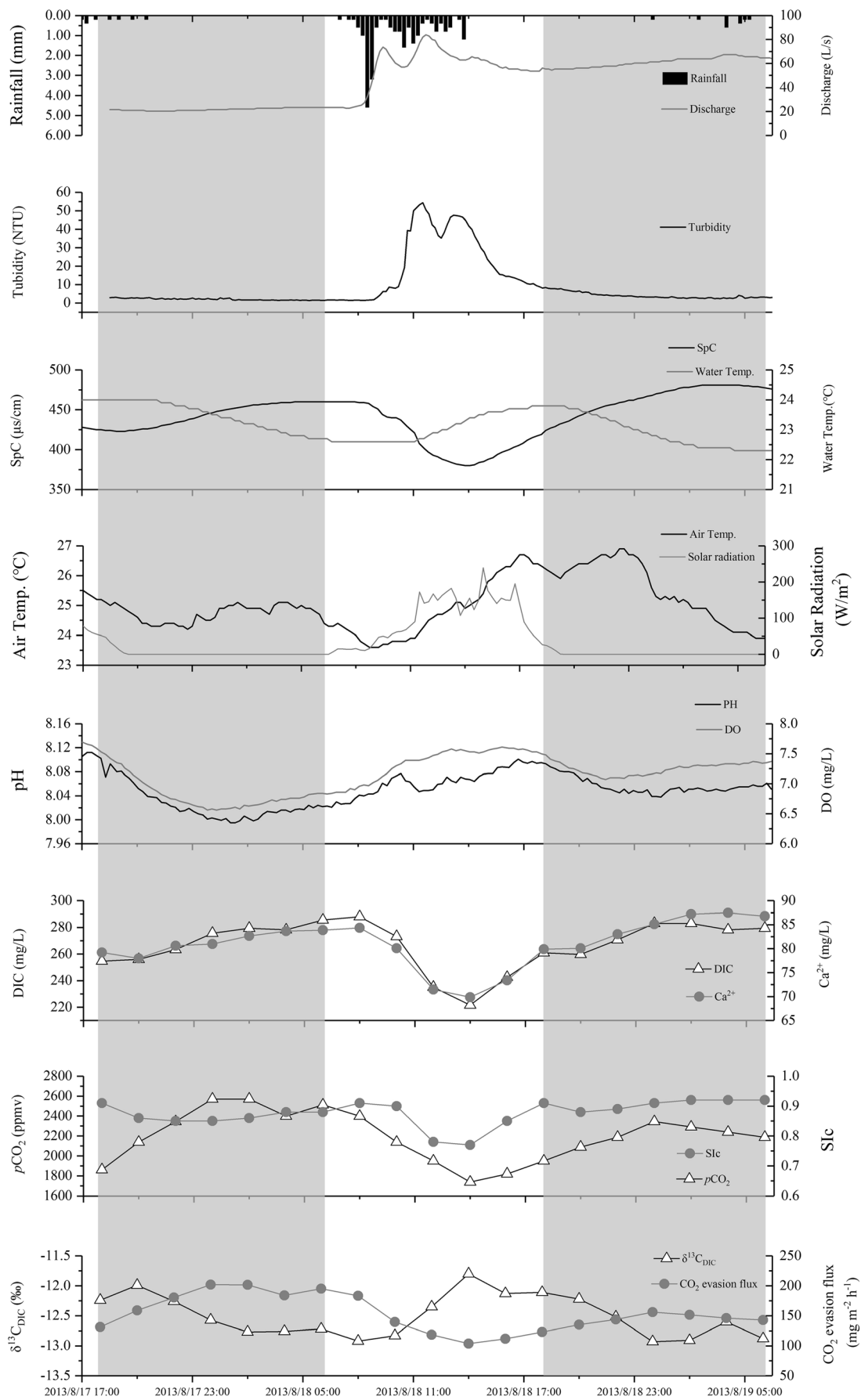
Fig. 2 Variation in rainfall, air temperature, solar radiation, stream discharge, hydrochemical parameters, $\delta^{13}\text{C}_{\text{DIC}}$, and CO_2 evasion flux at CK over 2 days from August 17 to 19, 2013. The spike of $\delta^{13}\text{C}_{\text{DIC}}$ in the

afternoon of August 18, 2013 may be caused by erroneous sampling or analyzing procedures

inverse correlation with pH and DO with minima occurring in the afternoon and maxima at night.

There was a significant decrease in the concentrations of DIC and Ca^{2+} between site CK and LY (Table S1, *t* test, $p < 0.001$). DIC and Ca^{2+} concentrations have diel patterns that are 180° out of phase with those of pH and DO at LY

(Fig. 3). DIC and Ca^{2+} concentrations increased to maximum values of 287.9 mg/L and 84.3 mg/L, respectively, at 0800 h on August 18. The peaks were followed by fast decline to afternoon lows of 221.6 mg/L and 69.9 mg/L, respectively at 1400 h (Fig. 3). The peak of discharge was consistent with the troughs of DIC and the Ca^{2+} time series. The water SIC



◀ **Fig. 3** Variation in rainfall, air temperature, solar radiation, stream discharge, turbidity, hydrochemical parameters, $\delta^{13}\text{C}_{\text{DIC}}$, and CO_2 evasion flux at LY over 2 days from August 17 to 19, 2013

values at LY were more than 0.7, reflecting greater supersaturation than at CK. The changing diel pattern of SiC at LY was similar with the curve of Ca^{2+} and DIC concentrations, with low values in the afternoon and high values occurring at night. The derived $p\text{CO}_2$ also showed a pronounced temporal change and was in phase with Ca^{2+} , DIC, and SiC (Fig. 3). The $p\text{CO}_2$ values at LY were significantly lower than at CK (Table S1, *t* test, $p < 0.01$). These results indicated that the diel cycles of hydrochemical parameters at LY still occurred during rain and increasing discharge events.

Variation in carbon isotope and CO_2 evasion flux

The range of measured $\delta^{13}\text{C}_{\text{DIC}}$ values in CK was -14.03 to -13.24‰ , with a mean of -13.74‰ ; although they a large range, the values show no regular diel pattern. The $\delta^{13}\text{C}_{\text{DIC}}$ values at LY were significantly higher than at CK (Table S1, $p < 0.003$) and vary from -12.93 to -11.80‰ . In contrast to CK, LY showed diel variations of $\delta^{13}\text{C}_{\text{DIC}}$ values with lower values at night and higher values in the afternoon. The $\delta^{13}\text{C}_{\text{DIC}}$ maxima at LY corresponded to DIC, Ca^{2+} , SpC , SiC , and $p\text{CO}_2$ minima and pH, DO, and water temperature maxima (Fig. 3). The $\delta^{13}\text{C}_{\text{DIC}}$ peaks also coincide roughly with the discharge and turbidity peaks but lagged about 2 h after discharge.

The difference of CO_2 evasion flux between CK and LY is also significant (Table S1, *t* test, $p = 0.000$). CO_2 evasion at CK varied from 1138.8 to 1505.3 $\text{mg}/\text{m}^2/\text{h}$ with a mean value of 1302.8 $\text{mg}/\text{m}^2/\text{h}$, which was about eight times higher than at LY, which ranged from 103.5 to 201.9 $\text{mg}/\text{m}^2/\text{h}$ with a mean value of 153.1 $\text{mg}/\text{m}^2/\text{h}$ (Table S1, Fig. 3).

CO_2 evasion did not show diel variation at the CK site over the study period, but it gradually decreased after the discharge and turbidity peaks ($Y = -259.58X + 10^7$, $R^2 = 0.70$, $p < 0.01$). The curve of CO_2 evasion at LY was smoother, and a diel pattern occurred with maxima at night that were about 1.3 times higher than during the daytime minima (Fig. 3). After the peaks of discharge and turbidity, CO_2 evasion decreased linearly at LY ($Y = -28.562X + 10^6$, $R^2 = 0.19$, $p < 0.01$). CO_2 evasion at LY was positively correlated with DIC, Ca^{2+} , and $p\text{CO}_2$ and inversely correlated with pH, DO, water temperature, and $\delta^{13}\text{C}_{\text{DIC}}$ (Fig. 3). These results also suggest that the diel cycles of carbon isotope and CO_2 evasion flux at LY still occur in the periods of rain and rising discharge.

Discussions

As diel frequency is an important timescale in this study, we focus on the data from 0600 h on August 18 to 0600 h on

August 19 to evaluate factors controlling DIC and to estimate the carbon budget relative to increased discharge related to a rain event.

Controls on carbon cycling

Rainwater can directly fall into the GSS channel and contribute to increased streamflow. The mean width of the water surface of the GSS was about 4.5 m during the study period. Although such a measurement has a large degree of uncertainty due to the limited information on channel width between two sites, it offered first-hand data for discussing the influence of rainwater. Regardless of the uncertainty in width, the measured regional rainfall into the GSS open channel contributed only about 1.9% of total discharge during the study period. Stream evapotranspiration will decrease water discharge (de Montety et al. 2011; Nimick et al. 2011). However, GUS discharge continuously increased after rain events during the study period, indicating that evapotranspiration was limited for influencing discharge variation. Therefore, in the following calculations and discussions, we neglect the influence of precipitation directly recharging into the GSS open channel and evapotranspiration on the chemical compositions of stream water (Nimick et al. 2011).

Because CK is located at the outlet of the GUS, its water source is groundwater and its hydrochemistry is controlled by the GUS karst system. The composition of this water was chemostatic throughout the study, yielding low CV values (Clow and Mast 2010; Karis et al. 2016). The lack of compositional variation resulted in weak correlations of DIC vs. $\delta^{13}\text{C}_{\text{DIC}}$, DIC vs. $p\text{CO}_2$, DIC vs. DO, DIC vs. CO_2 evasion flux, and DIC vs. discharge at CK at diel timescale (24 h) (Fig. 4a–i). Karst groundwater typically shows that the DIC and $\delta^{13}\text{C}_{\text{DIC}}$ originate from soil CO_2 produced by the degradation of organic matter and plant root respiration and the dissolution of carbonate minerals (Marx et al. 2017; Nimick et al. 2011; Tobias and Böhlke 2010). The chemostatic characteristics of DIC and $\delta^{13}\text{C}_{\text{DIC}}$ suggest that inorganic carbon at CK also originates from multiple invariant processes (carbonate rock dissolution and soil CO_2 hydration) in the subsurface as suggested during a seasonal (dry versus wet) study at this location (Zhang et al. 2017b).

In contrast to CK, LY showed significant correlations of DIC with $\delta^{13}\text{C}_{\text{DIC}}$, $p\text{CO}_2$, DO, CO_2 evasion flux, and discharge over the study period (Fig. 4a–i). These correlations suggest that other processes, in addition to soil- CO_2 production and carbonate rock dissolution, could affect water chemistry in the GSS. Commonly, varying temperature could decrease pH by increasing CO_2 evasion as water warms during the day (de Montety et al. 2011; Nimick et al. 2011; Spiro and Pentecost 1991). In Fig. 3, $p\text{CO}_2$ and CO_2 evasion were lower and DO concentration was higher during the day than at night at the LY site. Water temperature at LY showed weak positive

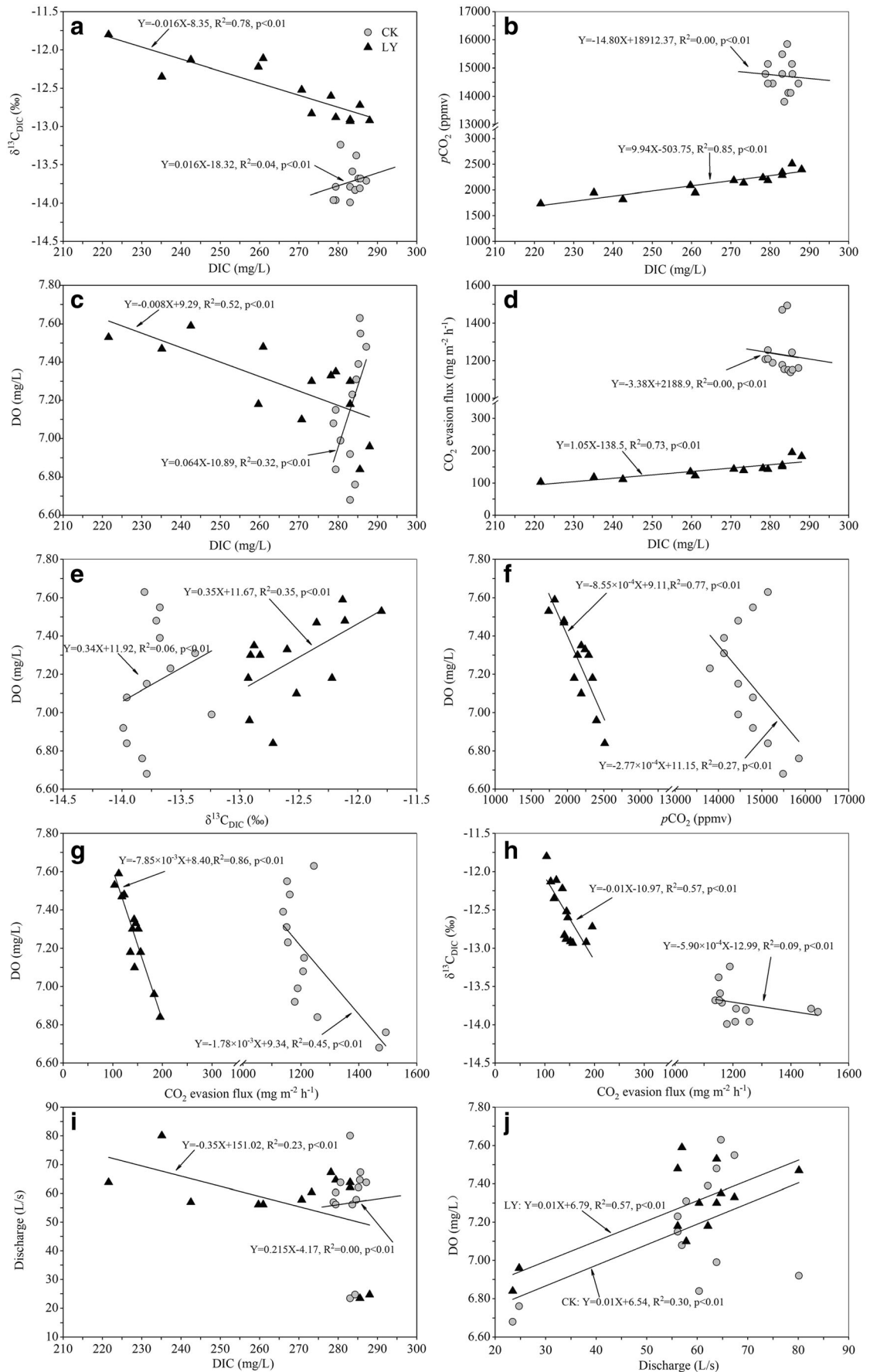


Fig. 4 Cross-plots between **a** $\delta^{13}\text{C}_{\text{DIC}}$ and DIC, **b** $p\text{CO}_2$ and DIC, **c** DO and DIC, **d** CO_2 evasion flux and DIC, **e** DO and $\delta^{13}\text{C}_{\text{DIC}}$, **f** DO and $p\text{CO}_2$, **g** DO and CO_2 evasion flux, **h** $\delta^{13}\text{C}_{\text{DIC}}$ and CO_2 evasion flux, **i** discharge and DIC, and **j** DO and discharge at extractive 24-h timescale from 0600 h on August 18 to 0600 h on August 19

correlations with DO concentration ($R^2 = 0.15$, $p < 0.01$; Fig. S1) and a slightly stronger negative correlation with CO_2 evasion ($R^2 = 0.34$, $p < 0.01$; Fig. S1). Moreover, DO concentrations showed a significant and strong negative correlation with both $p\text{CO}_2$ ($R^2 = 0.77$, $p < 0.01$; Fig. 4f) and CO_2 evasion ($R^2 = 0.86$, $p < 0.01$; Fig. 4g). Consequently, temperature does not appear to be the primary controlling factor on $p\text{CO}_2$ in the GSS. CO_2 evasion at LY should decrease DIC concentration, but a significant positive correlation occurred between water CO_2 evasion and DIC concentration ($R^2 = 0.73$, $p < 0.01$, Fig. 4d). Previous studies have demonstrated that CO_2 outgassing can increase $\delta^{13}\text{C}_{\text{DIC}}$ values in the residual DIC in water (Deirmendjian and Abril 2018; Doctor et al. 2008; Spiro and Pentecost 1991). However, LY shows a significant negative correlation between CO_2 evasion and $\delta^{13}\text{C}_{\text{DIC}}$ values ($R^2 = 0.57$, $p < 0.01$, Fig. 4h), suggesting that CO_2 outgassing is not the primary control of $\delta^{13}\text{C}_{\text{DIC}}$ values.

The diel cycle of DIC and DO concentrations is affected by in-stream metabolism in the GSS, including photosynthesis and respiration during sunny days with relatively stable and higher water level (Pu et al. 2017). These processes control DIC because photosynthesis releases O_2 into water and consumes CO_2 during the day, while respiration consumes O_2 and releases CO_2 into water during the night, making DO concentrations and $p\text{CO}_2$ ideal for evaluating aquatic metabolic process (de Montety et al. 2011; Demars et al. 2015; Kurz et al. 2013). The inverse variation of DIC with DO at LY (Fig. 4c) thus reflects in-stream metabolism even during overcast periods, changing discharge, decreased temperature, and increased turbidity during precipitation. Even with these limiting environmental condition, the rate of photosynthesis in the stream exceeded respiration during the day, causing a net release of O_2 and consumption of CO_2 , thereby increasing pH (Fig. 3). In contrast, respiration consumed O_2 and released CO_2 during the night thereby decreased the pH (Fig. 3). Therefore, metabolic processes are more important controls than temperature, turbidity, and discharge effects for DIC, $p\text{CO}_2$, and DO diel cycle in the GSS.

The $\delta^{13}\text{C}_{\text{DIC}}$ values in stream water are controlled by CO_2 sources (Marx et al. 2017). At LY, $\delta^{13}\text{C}_{\text{DIC}}$ has a positive correlation with DO concentrations ($R^2 = 0.35$, $p < 0.01$; Fig. 4e) and a significantly negative correlation with $p\text{CO}_2$ ($R^2 = 0.74$, $p < 0.01$; Fig. S1), reflecting in-stream metabolic controls on $\delta^{13}\text{C}_{\text{DIC}}$ values. This control results from a ^{13}C enrichment of residual pools of DIC during the day as DIC is consumed by photosynthesis and release of isotopically light biogenic CO_2 during nighttime due to respiration of organic

matter (Cavalli et al. 2012; Hasler et al. 2016; Pedersen et al. 2013; Zhao and Su 2014).

CO_2 evasion fluxes at both CK and LY decreased with the rising discharge (Figs. 2 and 3), although LY was characterized by a diel pattern. According to Eq. 4, increasing discharge will decrease the k_{600} value, causing a decrease in CO_2 evasion (Eq. 1). This decrease differs from CO_2 evasion from the Santa Fe River, FL, USA (Khadka et al. 2014), and the Madeira River, the largest tributary of the Amazon River, Brazil (Almeida et al. 2017), where flooding was found to enhance CO_2 evasion from water. However, CO_2 evasion increased at LY after maximum discharge. Daytime CO_2 evasion (mean = 129 $\text{mg}/\text{m}^2/\text{h}$) is about 15.1% lower than nighttime CO_2 evasion (mean = 152 $\text{mg}/\text{m}^2/\text{h}$) because of differences in the production and consumption of CO_2 during photosynthesis and respiration. Therefore, in-stream metabolism controls CO_2 evasion at LY. Our results show that diel variations in CO_2 evasion to atmosphere from streams and rivers should be taken account for a more accurate estimation of carbon budgets (Pu et al. 2017; Zhang et al. 2017a).

Although variations in stream discharge showed no relationship with DIC and DO concentrations (Fig. 4i, j) at CK, discharge had a negative relationship with DIC ($R^2 = 0.23$, $p < 0.01$, Fig. 4i) and a significantly positive relationship with DO ($R^2 = 0.57$, $p < 0.01$, Fig. 4j) at LY. We used a partial least-squares regression (PLS) model to evaluate to what extent discharge influences DIC diel variation at LY (Li et al. 2014; Paranaíba et al. 2018; Peter et al. 2014). PLS analyses included discharge, pH, SpC, DO, water temperature, DIC, Ca^{2+} , $\delta^{13}\text{C}_{\text{DIC}}$, $p\text{CO}_2$, and CO_2 evasion flux at LY only, using SIMCA 14.1 software (32-bit, Umetrics, Sweden). Due to a lack of any linear relationship between DIC, DO, and discharge, this PLS model did not analyze the data at CK. The PLS model performance is expressed in the terms R^2Y and Q^2 . R^2Y is comparable to R^2 in linear regression and expresses how much of the variance in Y is explained by the X variables. Q^2 is a measure of the predictive power of the PLS model. The model is more robust as Q^2 approaches R^2Y (Paranaíba et al. 2018; Peter et al. 2014; Sobek et al. 2003). Variable importance in projection (VIP) describes how much a variable contributes to explaining the Y variable (DIC). Highly important variables have $\text{VIP} > 1.0$, moderately important variables have $0.8 < \text{VIP} < 1.0$, and unimportant variables have $\text{VIP} < 0.8$. In this study, the PLS model explained the variability in DIC well, with a R^2Y of 0.99 and a Q^2 of 0.98 (Table S2). The PLS models show that SiC, Ca^{2+} , $p\text{CO}_2$, $\delta^{13}\text{C}_{\text{DIC}}$, CO_2 evasion flux, and DO were important variables ($\text{VIP} > 0.8$; Table S2) to explain DIC concentrations. However, discharge was less important ($\text{VIP} < 0.8$; Table S2), reflecting limited control by discharge for the DIC diel cycle at LY. Consequently, in-stream metabolism remained an important driver of the DIC diel cycle, even during rising discharge following precipitation and the overcast nature of the study period.

Carbon sink produced by in-stream metabolism

Lower DIC concentrations at LY compared to CK (Figs. 2 and 3, Table S1) reflect carbon losses. The loss represents the carbon sink produced by in-stream metabolism, which could be buried in benthic sediments similar to the oceanic biological pump (McElroy 1983) and would represent a net loss of atmospheric CO₂ to the sediments (Jiang et al. 2013; Liu et al. 2010, 2015; Liu and Dreybrodt 2015; Pu et al. 2017; Yang et al. 2015). A usual mass balance method was used to estimate the mass of carbon sink due to in-stream metabolism (de Montety et al. 2011; Liu et al. 2015; Liu and Dreybrodt 2015; Pu et al. 2017; Yang et al. 2015). The popular balance equation can be found below (Liu et al. 2015; Yang et al. 2015; Pu et al. 2017):

$$F_{OC} = \sum_i^t \left(\frac{\Delta \text{DIC}}{5.08} \right)_i \times Q_i - \sum_i^t \left(\frac{\Delta \text{Ca}}{3.337} \right)_i \times Q_i - \sum_i^t \left(\frac{F}{3.664} \right)_i \times A \quad (5)$$

where F_{OC} is the net mass of organic carbon formed in a day (mg/day), Q is the discharge of GS (L/s), ΔDIC is the amount of DIC loss between the CK and LY in each time step, 5.08 is a conversion factor between the molar mass of DIC and carbon (61.02/12.01), ΔCa is the amount of CaCO₃ lost between CK and LY in each time step, 3.337 is the conversion factor between the molar mass of calcium and carbon (40.08/12.01), F is the CO₂ evasion flux from unit water surface area (mg/m²/h), 3.664 is the conversion factor between the molar mass of CO₂ and carbon (44.01/12.01), and A is the GS water surface area during the study period (m²). The CO₂ evasion flux from upstream to downstream regions showed strong spatial heterogeneity; however, the measured DIC concentration at CK was stable, suggesting that CO₂ evasion flux cannot affect DIC concentrations at CK. Consequently, we use the evasion at LY for modeling. In Eq. 5, the first term on the right hand side of the equation denotes the total carbon loss/gain in GS over the study periods, the second term is the amount of carbon formed as calcite in GS, and the third term is the carbon loss via CO₂ evasion from the GS to the atmosphere.

These calculations show that the total carbon loss was 15.19 kg C/day and the amount of carbon formed as calcite was 4.34 kg C/day. The carbon loss via CO₂ evasion from the GS to the atmosphere was 5.21 kg C/day. Therefore, the carbon sink in the GSS channel produced by in-stream metabolism was around 5.6 kg C/day during the study period, which is about 6.1 times higher than it was in July, 2013 (sunny day, 0.91 kg C/day) (Pu et al. 2017). The result suggests that karst streams contribute to the terrestrial atmospheric carbon sink by stabilizing inorganic carbon originating from carbonate weathering process through the burial of organic carbon produced during aquatic photosynthesis (Liu and Dreybrodt 2015; Martin 2017; Pu et al. 2017).

Practical implications

Much work on diel cycles of inorganic and organic carbon in rivers, streams, and creeks occurs during sunny weather and stable water level, and much of it reflects that in-stream metabolism (photosynthesis and respiration) is the primary control of diel cycle of carbon (de Montety et al. 2011; Jiang et al. 2013; Liu et al. 2015; Parker et al. 2005, 2007, 2014; Pu et al. 2017; Tobias and Boehlke 2011; Yang et al. 2015). Our results suggest that even with overcast conditions, precipitation, rising discharge, and elevated turbidity, in-stream metabolism results in diel cycles of DIC due to weak solar radiation. Consequently, the carbon sink produced by in-stream metabolism can occur in karst streams regardless of variations in environmental conditions. Karst terrains cover around 14.7% of earth's surface (Chen et al. 2017), and most of headwater systems are sources of groundwater with elevated DIC concentrations. The stream outflows are also highly productive because of the generally clear water and solar radiation. The carbon sink produced by in-stream metabolism should be considered within the context of the global carbon cycle.

However, this study focuses only on a small subtropical stream fed by karst groundwater and a medium rainfall event (~22.8 mm) in summer. Additional similar studies in different climatic zones, land use types, rainfall events, and flow regimes could improve the understanding of the extent and causes of diel cycle of DIC.

Conclusions

This study demonstrates that overcast conditions, precipitation, and increased discharge and turbidity did not disrupt the diel cycle of DIC and carbon sink produced by in-stream metabolism (photosynthesis and respiration) in a karst headwater stream in southern China. Although diel conditions developed in ~1.3 km downstream of the chemostatic stream source, water chemistry showed significant diel variations. The variations resulted from metabolism of the submerged aquatic community and were not influenced by rainfall and rising discharge. Daytime photosynthesis caused a net release of O₂ and consumption of DIC that when buried in the sediment was sequestered; at night, respiration consumed O₂ and released CO₂, resulting in an increase of DIC. The estimated organic carbon sink by in-stream metabolism is around 5.6 kg C/day during the study period, indicating that the submerged aquatic community in a karst stream can significantly stabilize carbon originating from karst weathering processes. Further study is needed to better understand the carbon sink produced by in-stream metabolism in different karst streams covering different climatic zone and land use types and to consider the influences derived from rainfall event and flow regimes.

Acknowledgements Special thanks are given to Wen Liu and Xue Mo for their help in field and lab works. Heartfelt thanks are also given to Qiang Zhang for his YSI and ISCO autosampler instruments.

Funding information The study is financially supported by National Natural Science Foundation of China (No. 41572234, No. 41202185, No. 41702271), the Special Fund for Basic Scientific Research of Chinese Academy of Geological Sciences (YYWF201636), the Guangxi Natural Science Foundation (2016GXNSFCA380002, 2017GXNSFFA198006), the Geological Survey Project of CGS (DD20160305-03), and the Special Fund for Basic Scientific Research of Institute of Karst Geology (No. 2017006).

Compliance with ethical standards

Conflict of interest The authors declare that they have no conflict of interest.

Publisher's note Springer Nature remains neutral with regard to jurisdictional claims in published maps and institutional affiliations.

References

- Almeida RM, Pacheco FS, Barros N, Rosi E, Roland F (2017) Extreme floods increase CO₂ outgassing from a large Amazonian river. *Limnol Oceanogr* 62:989–999. <https://doi.org/10.1002/lno.10480>
- Atekwana EA, Krishnamurthy RV (1998) Seasonal variations of dissolved inorganic carbon and $\delta^{13}\text{C}$ of surface waters: application of a modified gas evolution technique. *J Hydrol* 205:265–278. [https://doi.org/10.1016/S0022-1694\(98\)00080-8](https://doi.org/10.1016/S0022-1694(98)00080-8)
- Atkins ML, Santos IR, Maher DT (2017) Seasonal exports and drivers of dissolved inorganic and organic carbon, carbon dioxide, methane and $\delta^{13}\text{C}$ signatures in a subtropical river network. *Sci Total Environ* 575:545–563. <https://doi.org/10.1016/j.scitotenv.2016.09.020>
- Cavalli G, Riis T, Baattrup-Pedersen A (2012) Bicarbonate use in three aquatic plants. *Aquat Bot* 98:57–60. <https://doi.org/10.1016/j.aquabot.2011.12.007>
- Chen Z et al (2017) The World Karst Aquifer Mapping project: concept, mapping procedure and map of Europe. *Hydrogeol J* 25:771–785
- Ciais P et al (2013) Carbon and other biogeochemical cycles. In: Stocker TF et al (eds) *Climate Change 2013: The Physical Science Basis. Contribution of Working Group I to the Fifth Assessment Report of the Intergovernmental Panel on Climate Change*. Cambridge University Press, Cambridge and New York, pp 465–570. <https://doi.org/10.1017/CBO9781107415324.015>
- Clow DW, Mast MA (2010) Mechanisms for chemostatic behavior in catchments: implications for CO₂ consumption by mineral weathering. *Chem Geol* 269:40–51. <https://doi.org/10.1016/j.chemgeo.2009.09.014>
- Covington MD (2016) The importance of advection for CO₂ dynamics in the karst critical zone: an approach from dimensional analysis. In: Feinberg JM, Gao Y, Alexander JEC (eds) *Caves and Karst Across Time*, vol Special Paper 516. Geological Society of America, pp 113–127. [https://doi.org/10.1130/2015.2516\(09\)](https://doi.org/10.1130/2015.2516(09))
- de Montety V, Martin JB, Cohen MJ, Foster C, Kurz MJ (2011) Influence of diel biogeochemical cycles on carbonate equilibrium in a karst river. *Chem Geol* 283:31–43. <https://doi.org/10.1016/j.chemgeo.2010.12.025>
- Deirmendjian L, Abril G (2018) Carbon dioxide degassing at the groundwater-stream-atmosphere interface: isotopic equilibration and hydrological mass balance in a sandy watershed. *J Hydrol* 558:129–143. <https://doi.org/10.1016/j.jhydrol.2018.01.003>
- Demars BOL, Thompson J, Manson JR (2015) Stream metabolism and the open diel oxygen method: principles, practice, and perspectives. *Limnol Oceanogr Methods* 13:356–374. <https://doi.org/10.1002/lom3.10030>
- Dinsmore KJ, Wallin MB, Johnson MS, Billett MF, Bishop K, Pumpanen J, Ojala A (2013) Contrasting CO₂ concentration discharge dynamics in headwater streams: a multi-catchment comparison. *J Geophys Res Biogeosci* 118:445–461. <https://doi.org/10.1002/jgrg.20047>
- Doctor DH, Kendall C, Sebestyen SD, Shanley JB, Ote N, Boyer EW (2008) Carbon isotope fractionation of dissolved inorganic carbon (DIC) due to outgassing of carbon dioxide from a headwater stream. *Hydrol Process* 22:2410–2423. <https://doi.org/10.1002/hyp.6833>
- Godsey SE, Kirchner JW, Clow DW (2009) Concentration-discharge relationships reflect chemostatic characteristics of US catchments. *Hydrol Process* 23:1844–1864. <https://doi.org/10.1002/hyp.7315>
- Gombert P (2002) Role of karstic dissolution in global carbon cycle. *Glob Planet Chang* 33:177–184. [https://doi.org/10.1016/S0921-8181\(02\)00069-3](https://doi.org/10.1016/S0921-8181(02)00069-3)
- Hasler CT, Butman D, Jeffrey JD, Suski CD (2016) Freshwater biota and rising pCO₂? *Ecol Lett* 19:98–108. <https://doi.org/10.1111/ele.12549>
- Hess JW, White WB (1988) Storm response of the karstic carbonate aquifer of southcentral Kentucky. *J Hydrol* 99:235–252
- Jiang ZC, Yuan DX (1999) CO₂ source-sink in karst processes in karst areas of China. *Episodes* 22:33–35
- Jiang Y, Hu Y, Schirmer M (2013) Biogeochemical controls on daily cycling of hydrochemistry and $\delta^{13}\text{C}$ of dissolved inorganic carbon in a karst spring-fed pool. *J Hydrol* 478:157–168. <https://doi.org/10.1016/j.jhydrol.2012.12.001>
- Johnson MS, Billett MF, Dinsmore KJ, Wallin M, Dyson KE, Jassal RS (2009) Direct and continuous measurement of dissolved carbon dioxide in freshwater aquatic systems—method and applications. *Ecology*:n/a. <https://doi.org/10.1002/eco.95>
- Karis T, Silvester E, Rees G (2016) Chemical regulation of alpine headwater streams during a storm event (Bogong High Plains, Victoria, Australia). *J Hydrol* 542:317–329. <https://doi.org/10.1016/j.jhydrol.2016.09.014>
- Khadka MB, Martin JB, Jin J (2014) Transport of dissolved carbon and CO₂ degassing from a river system in a mixed silicate and carbonate catchment. *J Hydrol* 513:391–402. <https://doi.org/10.1016/j.jhydrol.2014.03.070>
- Kurz MJ, de Montety V, Martin JB, Cohen MJ, Foster CR (2013) Controls on diel metal cycles in a biologically productive carbonate-dominated river. *Chem Geol* 358:61–74. <https://doi.org/10.1016/j.chemgeo.2013.08.042>
- Li Z, Zhang Z, Xiao Y, Guo J, Wu S, Liu J (2014) Spatio-temporal variations of carbon dioxide and its gross emission regulated by artificial operation in a typical hydropower reservoir in China. *Environ Monit Assess* 186:3023–3039. <https://doi.org/10.1007/s10661-013-3598-0>
- Liu Z, Dreybrodt W (2015) Significance of the carbon sink produced by H₂O-carbonate-CO₂-aquatic phototroph interaction on land. *Science Bulletin* 60:182–191. <https://doi.org/10.1007/s11434-014-0682-y>
- Liu Z, Zhao J (2000) Contribution of carbonate rock weathering to the atmospheric CO₂ sink. *Environ Geol* 39:1053–1058. <https://doi.org/10.1007/s002549900072>
- Liu Z, Chris G, Yuan D, Meiman J (2004) South China karst aquifer storm-scale hydrochemistry. *Ground water* 42:491–499
- Liu Z, Li Q, Sun H, Wang J (2007) Seasonal, diurnal and storm-scale hydrochemical variations of typical epikarst springs in subtropical karst areas of SW China: soil CO₂ and dilution effects. *J Hydrol* 337:207–223. <https://doi.org/10.1016/j.jhydrol.2007.01.034>
- Liu Z, Dreybrodt W, Wang H (2010) A new direction in effective accounting for the atmospheric CO₂ budget: considering the combined action of carbonate dissolution, the global water cycle and

- photosynthetic uptake of DIC by aquatic organisms. *Earth-Sci Rev* 99:162–172. <https://doi.org/10.1016/j.earscirev.2010.03.001>
- Liu H, Liu Z, Macpherson GL, Yang R, Chen B, Sun H (2015) Diurnal hydrochemical variations in a karst spring and two ponds, Maolan karst experimental site, China: biological pump effects. *J Hydrol* 522:407–417. <https://doi.org/10.1016/j.jhydrol.2015.01.011>
- Looman A, Santos IR, Tait DR, Webb JR, Sullivan CA, Maher DT (2016) Carbon cycling and exports over diel and flood-recovery timescales in a subtropical rainforest headwater stream. *Sci Total Environ* 550:645–657. <https://doi.org/10.1016/j.scitotenv.2016.01.082>
- Lynch JK, Beatty CM, Seidel MP, Jungst LJ, DeGrandpre MD (2010) Controls of riverine CO₂ over an annual cycle determined using direct, high temporal resolution pCO₂ measurements. *J Geophys Res Biogeosci* 115. <https://doi.org/10.1029/2009jg001132>
- Mann PJ, Spencer RGM, Dinga BJ, Poulson SR, Hernes PJ, Fiske G, Salter ME, Wang ZA, Hoering KA, Six J, Holmes RM (2014) The biogeochemistry of carbon across a gradient of streams and rivers within the Congo Basin. *J Geophys Res Biogeosci* 119:687–702. <https://doi.org/10.1002/2013jg002442>
- Martin JB (2017) Carbonate minerals in the global carbon cycle. *Chem Geol* 449:58–72
- Martin JB, Brown A, Ezell J (2013) Do carbonate karst terrains affect the global carbon cycle? *Acta Carsol* 42:187–196
- Martin JB, Kurz MJ, Khadka MB (2016) Climate control of decadal-scale increases in apparent ages of eogenetic karst spring water. *J Hydrol* 540:988–1001. <https://doi.org/10.1016/j.jhydrol.2016.07.010>
- Marx A, Dusek J, Jankovec J, Sanda M, Vogel T, van Geldern R, Hartmann J, Barth JAC (2017) A review of CO₂ and associated carbon dynamics in headwater streams: a global perspective. *Rev Geophys* 55:560–585. <https://doi.org/10.1002/2016rg000547>
- McElroy MB (1983) Marine biological-controls on atmospheric CO₂ and climate. *Nature* 302:328–329. <https://doi.org/10.1038/302328a0>
- Mo X (2015) Change processes and influence factors of dissolved inorganic carbon in a surface creek fed by a karst subterranean stream in subtropical karst area, SW China. Southwest University
- Nimick DA, Gammons CH, Parker SR (2011) Diel biogeochemical processes and their effect on the aqueous chemistry of streams: a review. *Chem Geol* 283:3–17. <https://doi.org/10.1016/j.chemgeo.2010.08.017>
- Paranaíba JR, Barros N, Mendonça R, Linkhorst A, Isidorova A, Roland F, Almeida RM, Sobek S (2018) Spatially resolved measurements of CO₂ and CH₄ concentration and gas-exchange velocity highly influence carbon-emission estimates of reservoirs. *Environ Sci Technol* 52:607–615. <https://doi.org/10.1021/acs.est.7b05138>
- Parker SR, Poulson SR, Gammons CH, DeGrandpre MD (2005) Biogeochemical controls on diel cycling of stable isotopes of dissolved O₂ and dissolved inorganic carbon in the big Hole River, Montana. *Environ Sci Technol* 39:7134–7140. <https://doi.org/10.1021/es0505595>
- Parker SR, Gammons CH, Poulson SR, DeGrandpre MD (2007) Diel variations in stream chemistry and isotopic composition of dissolved inorganic carbon, upper Clark Fork River, Montana, USA. *Appl Geochem* 22:1329–1343. <https://doi.org/10.1016/j.apgeochem.2007.02.007>
- Parker SR, Darvis MN, Poulson SR, Gammons CH, Stanford JA (2014) Dissolved oxygen and dissolved inorganic carbon stable isotope composition and concentration fluxes across several shallow floodplain aquifers and in a diffusion experiment. *Biogeochemistry* 117:539–552. <https://doi.org/10.1007/s10533-013-9899-0>
- Pedersen O, Colmer TD, Sand-Jensen K (2013) Underwater photosynthesis of submerged plants—recent advances and methods. *Front Plant Sci* 4:140. <https://doi.org/10.3389/fpls.2013.00140>
- Peter H, Singer GA, Preiler C, Chiffard P, Steniczka G, Battin TJ (2014) Scales and drivers of temporal pCO₂ dynamics in an Alpine stream. *J Geophys Res Biogeosci* 119:1078–1091. <https://doi.org/10.1002/2013jg002552>
- Pu J, Yuan D, Zhao H, Shen L (2014) Hydrochemical and PCO₂ variations of a cave stream in a subtropical karst area, Chongqing, SW China: piston effects, dilution effects, soil CO₂ and buffer effects. *Environ Earth Sci* 71:4039–4049
- Pu J, Li J, Khadka MB, Martin JB, Zhang T, Yu S, Yuan D (2017) In-stream metabolism and atmospheric carbon sequestration in a groundwater-fed karst stream. *Sci Total Environ* 579:1343–1355. <https://doi.org/10.1016/j.scitotenv.2016.11.132>
- Raymond PA, Zappa CJ, Butman D, Bott TL, Potter J, Mulholland P, Laursen AE, McDowell WH, Newbold D (2012) Scaling the gas transfer velocity and hydraulic geometry in streams and small rivers. *Limnol Oceanogr* 57:2:41–53. <https://doi.org/10.1215/21573689-1597669>
- Rice EW, Baird RB, Eaton AD, Clesceri LS (2012) Standard methods for the examination of water and wastewater, 22nd edn. American Public Health Association, the American Water Works Association and the Water Environment Federation, Washington D.C
- Shin WJ, Chung GS, Lee D, Lee KS (2011) Dissolved inorganic carbon export from carbonate and silicate catchments estimated from carbonate chemistry and δ¹³C_{DIC}. *HESS* 15:2551–2560. <https://doi.org/10.5194/hess-15-2551-2011>
- Shuster ET, White WB (1971) Seasonal fluctuations in the chemistry of lime-stone springs: a possible means for characterizing carbonate aquifers. *J Hydrol* 14:93–128
- Sobek S, Algesten G, Bergstrom AK, Jansson M, Tranvik LJ (2003) The catchment and climate regulation of pCO₂ in boreal lakes. *Glob Chang Biol* 9:630–641
- Spiro B, Pentecost A (1991) One day in the life of a stream—a diurnal inorganic carbon mass balance for a travertine-depositing stream (waterfall beck, Yorkshire). *Geomicrobiol J* 9:1–11. <https://doi.org/10.1080/01490459109385981>
- Tobias C, Boehlke JK (2011) Biological and geochemical controls on diel dissolved inorganic carbon cycling in a low-order agricultural stream: implications for reach scales and beyond. *Chem Geol* 283:18–30. <https://doi.org/10.1016/j.chemgeo.2010.12.012>
- Tobias C, Böhlke JK (2010) Biological and geochemical controls on diel dissolved inorganic carbon cycling in a low-order agricultural stream: implications for reach scales and beyond. *Chem Geol*. <https://doi.org/10.1016/j.chemgeo.2010.12.012>
- Vesper D, White W (2003a) Storm pulse chemographs of saturation index and carbon dioxide pressure: implications for shifting recharge sources during storm events in the karst aquifer at Fort Campbell, Kentucky/Tennessee, USA. *Hydrogeol J* 12. <https://doi.org/10.1007/s10040-003-0299-8>
- Vesper DJ, White WB (2003b) Metal transport to karst springs during storm flow: an example from Fort Campbell, Kentucky/Tennessee, USA. *J Hydrol* 276:20–36. [https://doi.org/10.1016/s0022-1694\(03\)00023-4](https://doi.org/10.1016/s0022-1694(03)00023-4)
- Vesper DJ, White WB (2004) Storm pulse chemographs of saturation index and carbon dioxide pressure: implications for shifting recharge sources during storm events in the karst aquifer at Fort Campbell, Kentucky/Tennessee, USA. *Hydrogeol J* 12:135–143
- Wigley TML (1977) WATSPEC: a computer program for determining the equilibrium speciation of aqueous solutions. Geo-Abstracts for the British Geomorphological Research Group
- Yang R, Chen B, Liu H, Liu Z, Yan H (2015) Carbon sequestration and decreased CO₂ emission caused by terrestrial aquatic photosynthesis: insights from diel hydrochemical variations in an epikarst spring and two spring-fed ponds in different seasons. *Appl Geochem* 63:248–260. <https://doi.org/10.1016/j.apgeochem.2015.09.009>
- Yuan D (1997) The carbon cycle in karst. *Z Geomorphol, Zeitschrift für Geomorphologie* 108(Suppl):91–102
- Zeng C, Liu ZH, Zhao M, Yang R (2016) Hydrologically-driven variations in the karst-related carbon sink fluxes: insights from high-resolution monitoring of three karst catchments in Southwest China. *J Hydrol* 533:74–90

- Zhang C, Wang J, Pu J, Yan J (2012) Bicarbonate daily variations in a karst river: the carbon sink effect of subaquatic vegetation photosynthesis. *Acta Geol Sin (Engl Ed)* 86:973–979. <https://doi.org/10.1111/j.1755-6724.2012.00721.x>
- Zhang T, Li J, Pu J, Martin JB, Khadka MB, Wu F, Li L, Jiang F, Huang S, Yuan D (2017a) River sequesters atmospheric carbon and limits the CO₂ degassing in karst area, southwest China. *Sci Total Environ* 609:92–101. <https://doi.org/10.1016/j.scitotenv.2017.07.143>
- Zhang T, Pu J, Li J, Yuan D, Li L (2017b) Stable isotope and aquatic geochemistry of a typical subtropical karst subterranean stream in southwest China. *Carbonates Evaporites* 32:415–430. <https://doi.org/10.1007/s13146-017-0356-3>
- Zhao B, Su Y (2014) Process effect of microalgal-carbon dioxide fixation and biomass production: a review. *Renew Sust Energ Rev* 31:121–132. <https://doi.org/10.1016/j.rser.2013.11.054>